

1 **Title:** Experimental determination of magnesi~~um~~ and silica solubilities in graphite-saturated and redox-
2 buffered high-pressure COH fluids in equilibrium with forsterite + enstatite and magnesite + enstatite

3
4 **Authors:** Tiraboschi C.^{1*}, Tumiati S.², Sverjensky D.³, Pettke T.⁴, Ulmer P.⁵, Poli S.²

5 ¹ Dipartimento di Scienze dell'Ambiente e della Terra, Università degli Studi di Milano Bicocca, piazza
6 della Scienza 4, 20126 Milano, Italy

7 ² Dipartimento di Scienze della Terra, Università degli Studi di Milano, via Mangiagalli 34, 20133
8 Milano, Italy

9 ³ Department of Earth & Planetary Sciences, Johns Hopkins University, 301 Olin Hall, 3400 N. Charles
10 Street, Baltimore, MD 21218, USA

11 ⁴ Institute of Geological Sciences, University of Bern, Baltzerstrasse 1+3, 3012 Bern, Switzerland

12 ⁵ Institute of Geochemistry and Petrology, ETH Zürich, Clausiusstrasse 25 / NW E77, 8092 Zürich,
13 Switzerland

14
15 *corresponding author: Carla Tiraboschi, email: carla.tiraboschi@unimib.it, Tel: +39 02 6448 2012

16
17 **Keywords:** mantle minerals solubility, ~~COH fluids~~carbon, ~~high pressure~~experimental petrologys, piston
18 -cylinder, cryogenic LA-ICP-MS

19
20 **Abstract**

21 We experimentally investigated the dissolution of forsterite, enstatite and magnesite in graphite-saturated
22 COH fluids synthesized using a rocking piston cylinder apparatus at pressures from 1.0 to 2.1 GPa and
23 temperatures from 700 to 1200 °C. Synthetic forsterite, enstatite, and ~~natural~~nearly pure ~~natural~~
24 magnesite were used as starting materials. ~~Redox conditions were buffered by Ni-NiO-H₂O, employing a~~
25 ~~double-capsule setting. Fluids, binary H₂O-CO₂ mixtures at the P, T, fO₂ conditions investigated, were~~
26 ~~generated from graphite, oxalic acid anhydrous (H₂C₂O₄) and water. Their dissolved solute loads were~~
27 ~~analyzed through an improved version of the cryogenic technique, which takes into account the~~
28 ~~complexities associated with the presence of CO₂-bearing fluids. Redox conditions were buffered by Ni-~~
29 ~~NiO-H₂O, employing a double-capsule setting. Carbon saturated COH fluids were generated from~~

Formattato: Italiano (Italia)

Formattato: Pedice

30 graphite, oxalic acid anhydrous ($\text{H}_2\text{C}_2\text{O}_4$) and water (doped with 580 ppm of Cs). A diamond powder
31 layer was employed to trap fluids with their dissolved solute loads, which were analyzed via cryogenic
32 laser ablation ICP-MS.

33 The experimental data show that forsterite + enstatite solubility in $\text{H}_2\text{O}-\text{CO}_2$ fluids ~~results in~~ higher
34 compared to pure water both in terms of dissolved silica SiO_2 solubility values ($m\text{SiO}_2 = 1.24 \text{ mol/kg}_{\text{H}_2\text{O}}$
35 vs. $m\text{SiO}_2 = 0.22 \text{ mol/kg}_{\text{H}_2\text{O}}$ at $P = 1 \text{ GPa}$, $T = 800 \text{ }^\circ\text{C}$) compared to the solubility in pure H_2O ($m\text{SiO}_2 =$
36 $0.22 \text{ mol/kg}_{\text{H}_2\text{O}}$ at $P = 1 \text{ GPa}$, $T = 800 \text{ }^\circ\text{C}$). Moreover, the presence of CO_2 also promotes the formation of
37 Mg-solutes and magnesia ($m\text{MgO} = 1.08 \text{ mol/kg}_{\text{H}_2\text{O}}$ vs. $m\text{MgO} = 0.28 \text{ mol/kg}_{\text{H}_2\text{O}}$ at $P = 1 \text{ GPa}$, $T = 800$
38 $^\circ\text{C}$), at levels much higher than in C-free systems ($m\text{MgO} = 0.28 \text{ mol/kg}_{\text{H}_2\text{O}}$ at $P = 1 \text{ GPa}$, $T = 800 \text{ }^\circ\text{C}$)
39 probably due to the formation of organic C-, Mg- and Si-bearing complexes. Compared to forsterite +
40 enstatite dissolution, magnesite dissolution in $\text{H}_2\text{O}-\text{CO}_2$ fluids results in lower MgO-magnesia
41 solubility values contents compared to forsterite dissolution ($m\text{MgO} = 0.41 \text{ mol/kg}_{\text{H}_2\text{O}}$ at $P = 1.5 \text{ GPa}$, T
42 $= 800 \text{ }^\circ\text{C}$) and its behavior molalities that strongly resembles those associated with calcite solubility in
43 pure water H_2O in terms of dissolved cations.

44 Our experimental results show that at low temperature conditions a graphite saturated $\text{H}_2\text{O}-\text{CO}_2$
45 fluid interacting with a simplified model mantle composition can lead to the formation of significant
46 amounts of enstatite, while at higher temperatures, this fluid seems to be less effective in metasomatize
47 the surrounding forsterite. COH fluids could represent an effective carrier of C-, Mg- and Si-bearing
48 species from the mantle wedge to shallowest level in the upper mantle.

49

50 1. Introduction

51 High-pressure aqueous fluids are able to transport significant amounts of dissolved species
52 (Manning 1994) derived from interaction with rock-forming minerals. Experimental constraints on the
53 extent of mineral dissolution are therefore crucial to understand metasomatic processes closely related to
54 the mass transport of elements by high-pressure fluids. For example, quartz dissolution in H_2O at
55 pressures and temperatures ranging from 0.1 to 2.0 GPa and 500 to 900 $^\circ\text{C}$ shows an increase of the total
56 dissolved silica ($\text{SiO}_{2,\text{aq}}$) in H_2O with increasing P and T (Anderson and Burnham 1965; Manning 1994).
57 The amount of solutes deriving from the dissolution of mantle minerals such as forsterite and enstatite
58 mobilized by high-pressure fluids has been also extensively investigated in H_2O -only systems

Formattato: Rientro: Prima riga: 1,25 cm

Formattato: Pedice

59 containing ~~only~~ pure water as volatile component (Nakamura and Kushiro 1974; Ryabchikov et al. 1982;
60 Manning and Boettcher 1994; Zhang and Frantz 2000; Newton and Manning 2002). Experimental
61 evidence indicated that lower amounts of dissolved silica ~~solves results in~~ from the dissolution of Mg-
62 silicates (forsterite, enstatite) ~~bearing systems compared to~~ than in the SiO₂-H₂O system ~~compared to the~~
63 dissolution of quartz.

64 For fluids bearing volatile carbon species in addition to water, several authors ~~In the system~~
65 SiO₂-H₂O-CO₂ mixed fluids show (e.g., Newton and Manning 2000) investigated the dissolution of
66 quartz in H₂O-CO₂ fluids showing decreasing amounts of SiO_{2,aq} with increasing content of CO₂ in the
67 fluid (e.g., Newton and Manning 2000). However, the effect of CO₂ addition to aqueous fluids in
68 equilibrium with mantle minerals has remained experimentally unexplored, ~~particularly under more~~
69 ~~reducing conditions in equilibrium with graphite~~, even though carbon dioxide is thought to be a
70 significant volatile species in ~~subduction-related~~ subduction-related fluids ~~occurring in the slab-mantle~~
71 ~~interface~~ (Tumiati et al., 2017).

72

73 1.1 Forsterite and enstatite solubility in H₂O

74 In early studies of silicate solubilities in aqueous fluids in the MgO-SiO₂-MgO (MSH) system,
75 at deep crustal and upper mantle conditions ($P < 2$ GPa and $T < 1300^{\circ}\text{C}$), the composition of the fluid
76 ~~phase was has been derive~~ estimated from phase relations projected to the H₂O-SiO₂ subsystem,
77 assuming that the amount of MgO in the fluid was negligible at the investigated condition (Nakamura and
78 Kushiro 1974; Ryabchikov et al. 1982; Zhang and Frantz 2000). ~~At deep crustal and upper mantle~~
79 conditions ($P < 2$ GPa and $T < 1300^{\circ}\text{C}$) the solubility of forsterite and enstatite in H₂O was investigated
80 first by Nakamura and Kushiro (1974). ~~At 1.5 GPa and temperatures from 1280 to 1340 °C who retrieved~~
81 the composition of the fluid phase at $P = 1.5$ GPa and $T = 1280 - 1340^{\circ}\text{C}$ from the location of phase
82 boundaries in the system MgO-SiO₂-H₂O (MSH) and projected to the H₂O-SiO₂ subsystem axis,
83 assuming that MgO concentration in the fluid was negligible at the investigated condition. The authors
84 ~~observed that an~~ aqueous fluids in equilibrium ~~saturated~~ with forsterite and enstatite ~~was~~ are able to
85 dissolve a significant amounts of SiO₂ ranging from ~~the~~ 18 wt.% at 1280 °C to ~~the~~ 22 wt.% at 1310 °C
86 (Nakamura and Kushiro 1974). At 3 GPa and 1000 °C the Mg/Si ratio increases with pressure and

Formattato: Pedice

Formattato: Pedice

Formattato: Pedice

Formattato: Pedice

Formattato: Pedice

Formattato: Pedice

87 reaches unity at 3 GPa and 1000 °C in a fluid containing > 30 wt.% of silicate solutes dissolved silica
88 (Ryabchikov et al. 1982).-

89 ~~———— Ryabchikov et al. (1982) and Zhang and Frantz (2000) extended the *PT* range of the~~
90 ~~study of Nakamura and Kushiro (1974) to 3 GPa and 1 to 2 GPa respectively, and lower temperatures (*T*~~
91 ~~= 900–1200 °C) using the same technique to estimate fluid composition. Ryabchikov et al. (1982)~~
92 ~~observed that in the MSH system, the Mg/Si ratio slightly increases with pressure, reaching 1 at 3 GPa~~
93 ~~and 1000 °C, where the fluid contains more than the 30 wt.% of silicates. Moreover, Zhang and Frantz~~
94 ~~(2000), highlighted that the thermodynamic properties of aqueous silica derived from silica saturated~~
95 ~~systems may not be applicable to calculation in silica-deficient systems at high-pressure conditions, due~~
96 ~~to the formation of silica dimers.~~

97 Another approach to quantify the amount of solutes was to extract both fluids and precipitates
98 from piston-cylinder experiments (Manning and Boettcher 1994). ~~different experimental approach was~~
99 ~~used by Manning and Boettcher (1994), who developed a device to extract both fluids and precipitates~~
100 ~~from piston-cylinder experiments. The solution was then analyzing them~~ by means of inductively
101 coupled plasma (ICP)-mass spectrometry (ICP-MS). Experimental data showed that at ~~the investigated~~
102 ~~conditions (*P* = 1–3 GPa and *T* = 700–1310 °C) the concentration of MgO in the solution was negligible~~
103 ~~(< 0.005 mol/kg_{H2O} = 200 ppm) compared to the SiO₂ content in the aqueous fluid (*m*SiO₂ = 0.071~~
104 ~~mol/kg_{H2O} at *P* = 1 GPa and *T* = 700 °C).~~

105 ~~Subsequently With a third approach, Newton and Manning (2002) applied the weight loss~~
106 ~~technique (Newton and Manning 2002), to measure the solubilities of forsterite + enstatite were~~
107 ~~measured from 0.4 to 1.5 GPa and from *T* = 700–900 °C. Silica concentrations at 1 GPa increase from~~
108 ~~0.16 mol/kg_{H2O} at 700 °C to 0.5 mol/kg_{H2O} at 900 °C, showing a small increase with pressure between 0.7~~
109 ~~and 1.4 GPa. The higher solubility data compared to those of Zhang and Frantz (2000) (0.34 mol/kg at 1~~
110 ~~GPa and 900 °C) were attributed by Newton and Manning (2002) to the quenching method employed by~~
111 ~~Zhang and Frantz (2000). It was suggested that decreasing temperature at nearly constant pressure could~~
112 ~~lead to the formation of hydrothermal enstatite, as the *P, T* path during quenching passed through the~~
113 ~~stability field of enstatite. The presence of enstatite having formed upon quench could have caused a~~
114 ~~misinterpretation of phase equilibrium boundaries by Zhang and Frantz (2000) leading to slightly~~
115 ~~underestimation of the silica content of the fluid.~~

Formattato: Rientro: Prima riga: 1,25 cm

Formattato: Pedice

Formattato: Pedice

Formattato: Tipo di carattere: Corsivo

Formattato: Pedice

116 ~~Finally, S. Kawamoto et al. (2004a) employed an externally heated diamond anvil cell (DAC)~~
117 ~~and synchrotron X-ray fluorescence spectroscopy (S-XRF), coupled with an externally heated diamond~~
118 ~~anvil cell (DAC), was employed to investigate enstatite and forsterite solubility in aqueous fluids from~~
119 ~~0.5 to 5.8 GPa and 800–1000 °C (Kawamoto et al. 2004a). At 3 GPa and 1000 °C it was observed that the~~
120 ~~authors observed that the Mg/Si ratio changes rapidly from SiO₂-rich to MgO-rich fluid, attributing this~~
121 ~~effect to probably due to possible structural changes in liquid water (Kawamoto et al. 2004b).~~

122 ~~Dissolution of solids in aqueous fluids generally increases with increasing *P*. At higher pressure~~
123 ~~conditions, the diamond trap technique (Baker and Stolper 1994; Ryabchikov et al. 1989) has been~~
124 ~~employed to trap precipitates and melt in a diamond-powder layer placed in the experimental capsule and~~
125 ~~subsequently analyzed via LA-laser ablation ICP-MS (LA-ICP-MS). For example, at 6 to 10.5 GPa and~~
126 ~~temperatures from 900 to 1200 °C in the MSH system, Stalder et al. (2001) employed a diamond powder~~
127 ~~layer in the experimental capsule (Baker and Stolper 1994) to trap precipitates and melt that are~~
128 ~~subsequently measured via LA-ICP-MS. Melekhova et al. (2007) Employing this technique determined~~
129 ~~the MSH system was investigated from 6 to 10.5 GPa and temperatures from 900 to 1200 °C (Stalder et~~
130 ~~al. 2001) and the second critical endpoint was located in the MSH system to be above 11 GPa~~
131 ~~(Melekhova et al. (2007) employing an improved version of the diamond trap technique, where the~~
132 ~~diamond layer is kept frozen during the LA-ICP-MS analyses, below which minerals coexist with an~~
133 ~~aqueous fluid below the system's water-saturated solidus, and the total dissolved fluid load was~~
134 ~~determined by cryogenic LA-ICP-MS (freezing technique; (Kessel et al. 2004; 2005a; 2005b). Using the~~
135 ~~same technique, also known as the freezing technique, (Kessel et al. (2005a; Kessel et al. 2005b)~~
136 ~~quantified the total dissolved load of the aqueous fluid across the second critical endpoint in the~~
137 ~~potassium-free basalt–H₂O system from 4–6 GPa.~~

Formattato: Non Evidenziato

138

139 1.2 Carbonate solubility in H₂O

140 Carbonate dissolution in H₂O has been investigated experimentally by several authors (Walther
141 and Long 1986; Fein and Walther 1989; Caciagli and Manning 2003; Sanchez-Valle et al. 2003). ~~The~~
142 ~~weight loss technique (Manning 1994) was employed to. Caciagli and Manning (2003) investigated the~~
143 ~~dissolution of calcite in pure H₂O-water up to *P* = 1.6 GPa and *T* = 500–900 °C (Caciagli and Manning~~
144 ~~2003) through the weight loss technique (Manning 1994) extending the pressure range of previous calcite~~

145 solubility studies (e.g., Fein and Walther 1989). Results indicate that the solubility of calcite at 1 GPa
146 increases with increasing temperature from 0.016 mol/kg at 500 °C to 0.057 mol/kg to 750 °C.

147 ~~The first experimental dataset on carbonate solubility at pressure greater than 2.0 GPa up to 3.6~~
148 ~~GPa and low temperature conditions ($T = 250$ °C) (Sanchez-Valle et al. 2003) investigated strontianite~~
149 ~~dissolution in H₂O was retrieved employing an externally heated DAC and synchrotron X-ray~~
150 ~~fluorescence spectroscopy up to 3.6 GPa and 250 °C (Sanchez-Valle et al. 2003), employing an externally~~
151 ~~heated DAC and S-XRF.~~

152 ~~In addition, a~~ significant effort has been made to develop thermodynamic models to predict
153 carbonate behavior in aqueous fluids (Dolejs and Manning 2010; Pan et al. 2013; Facq et al. 2014; Pan
154 and Galli 2016). ~~Facq et al. (2014) presented an integrated experimental and theoretical study of aragonite~~
155 ~~solubility in an aqueous fluid from 0.5 to 8 GPa and 300 to 400 °C.~~ Results indicate that HCO₃⁻ is the
156 dominant species ~~from aragonite dissolution in an aqueous fluids dissolving aragonite~~ below 4 GPa ~~and~~
157 ~~low temperature conditions (300–400 °C)~~, while at higher pressures CO₃²⁻ becomes the dominant species,
158 in contrast ~~with to~~ the previously hypothesized predominance of CO_{2,aq} in aqueous fluids (~~Facq et al.~~
159 ~~(2014). Moreover, accordingly to theoretical calculations, Pan et al. (2013) predicted the solubility of~~
160 ~~different carbonate minerals, showing that~~ magnesite, insoluble in water at ambient condition, becomes
161 ~~slightly~~ soluble at 10 GPa (Pan et al. 2013).

162

163 1.3 Solubilities in COH mixed H₂O–CO₂ fluids

164 ~~So far, the amount of solutes mobilized by high-pressure fluids has been mainly investigated in~~
165 ~~CO₂-free aqueous systems even though CO₂ is considered a significant volatile in subduction-related~~
166 ~~fluids. In particular, the effect of CO₂ addition to aqueous fluids in equilibrium with mantle minerals~~
167 ~~remains experimentally unexplored.~~ Experimental data on mineral dissolution in mixed H₂O–CO₂ fluid
168 are available only for quartz (Walther and Orville 1983; Newton and Manning 2000; Shmulovich et al.
169 2006; Newton and Manning 2009), albite and diopside (Shmulovich et al. 2001) and suggests that the
170 presence of CO₂ lowers the solute content in the fluid by lowering the ~~silica-water~~ activity (~~i.e., by~~
171 ~~increasing the CO₂ content~~).

172 ~~To analyze the solubility of quartz in CO₂–H₂O mixed fluids,~~ Walther and Orville (1983)
173 developed an extraction quench-hydrothermal apparatus ~~to analyze the solubility of quartz in extracted~~

Formattato: Rientro: Prima riga: 1,25 cm

Formattato: Tipo di carattere: Corsivo

Formattato: Evidenziato

Formattato: Pedice

Formattato: Pedice

Formattato: Pedice

174 ~~CO₂-H₂O mixed fluids~~. In these experiments, performed in cold seal vessels, the pressure was limited to
175 0.2 GPa at $T < 600$ °C. ~~The authors observed a~~Results show a decrease in quartz solubility ~~by with~~
176 increasing ~~the amounts~~ of CO₂ in the ~~COH~~-fluid.

177 ~~Concerning P - T conditions similar to our experimental study, Another option is to~~ ~~The collected~~
178 ~~solutes extract and collect the solutes~~ed from the ~~capsule~~piston cylinder experiments. Solute~~s~~ ~~were mixed~~
179 ~~with LiBO₂ and fused in graphite capsule at $T = 1000$ °C for 10 minutes (Schneider and Eggler 1986)~~.
180 ~~WDS analyses~~Glasses were then analyzed ~~performed employing using the an electron microprobe~~.
181 ~~T~~Schneider and Eggler (1986) investigated the solubility of different types of peridotites (amphibole,
182 phlogopite- and ~~clinopyroxene-bearing~~jadeite peridotites) and single minerals in mixed H₂O-CO₂ fluids
183 ~~were retrieved~~ at $P = 1.5$ - 2 GPa and $T = 600$ - 1100 °C. ~~The collected solutes extracted from the capsule~~
184 ~~were mixed with LiBO₂ and fused in graphite capsule at $T = 1000$ °C for 10 minutes. WDS analyses were~~
185 ~~performed employing the electron probe~~. ~~The authors observed~~Results show that the addition of CO₂ (9
186 mol%) to the aqueous fluid strongly ~~depressed~~-depresses the solubility of silicates by approximately one
187 order of magnitude.

188 ~~A modified version of the weight loss technique was employed to~~ Aranovich and Newton (1999)
189 determined activity-composition relations in CO₂-H₂O solutions (Aranovich and Newton 1999)~~by~~
190 ~~modifying the weight loss technique~~. The capsule was frozen in liquid nitrogen and punctured with a
191 needle while still frozen. The immediate weight loss ~~was~~ ascribed to CO₂ escape. The capsules were then
192 dried and reweighed to retrieve the H₂O content. This technique, ~~applied on double capsules, that~~ was
193 also ~~considered used later by~~ Newton and Manning (2000; 2009), ~~two~~ who investigated quartz dissolution in
194 H₂O-CO₂ at $P = 0.2$ - 1.5 GPa and $T = 500$ - 900 °C (Newton and Manning 2000; 2009)~~using the puncture~~
195 ~~weight loss technique applied on double capsules~~. The amount of solubility of SiO₂ in the fluid decreases
196 strongly with increasing CO₂, in agreement with previous experimental data.

197

198 2. Experimental

199 2.1 Starting materials

200 Carbon-saturated ~~COH-H₂O-CO₂~~ fluids were generated starting from oxalic acid anhydrous
201 (OAA; H₂C₂O₄), ~~H₂O-water~~ and glassy carbon spherical powder (grain size 80-200 μm). The thermal
202 dissociation of OAA at $T > 600$ °C generates a CO₂-H₂ fluid according to reaction:

Formattato: Pedice

Formattato: Pedice



204 ~~As an internal standard for LA-ICP-MS data quantification (Kessel et al. 2004), the H₂O was doped with~~
205 ~~585 µg/g of cesium [Cs(OH)₂] and the Cs concentration was checked by means of ICP-MS. The addition~~
206 ~~of a known amount of Cs-doped H₂O water, added to in the capsule through a microsyringe, alloweds to~~
207 obtain a roughly equimolar CO₂-H₂O starting ~~mixture-fluid phase~~ with $X_{\text{CO}_2} [= \text{CO}_2 / (\text{H}_2\text{O} + \text{CO}_2)] = 0.5$.

208 ~~As an internal standard for LA-ICP-MS data quantification (see Kessel et al. 2004), the H₂O water was~~
209 ~~doped with 585 µg/g of cesium [Cs(OH)₂] and the Cs concentration was checked by liquid mode ICP-MS.~~

210 Two ~~mineral assemblages different starting materials~~ were considered: (i) a mixture of forsterite
211 and minor enstatite (FoEn) and (ii) a mixture of enstatite, magnesite and minor forsterite (EnMgs).
212 Forsterite and enstatite were synthesized from dried nano-crystalline Mg(OH)₂ (Sigma-Aldrich, 99.9%
213 purity) and silicon dioxide (Balzers, 99.9% purity), mixed in stoichiometric proportions, pelletized and
214 loaded in a vertical furnace at 1500 °C for 24 h. Synthesis products were ground in ethanol for 1 hour,
215 dried and characterized by X-ray powder diffraction analysis (Bruker, AXS D8 Advance, ETH Zurich;
216 Philips X'pert MPD, University of Milan). Natural magnesite from Pinerolo (Italy), checked for ~~impurity~~
217 ~~and characterized~~ through electron ~~microscopy and microprobe analyses~~ (Jeol 8200 Superprobe,
218 University of Milan), was ground under ethanol for 1 h and dried. The resulting composition of the
219 mixtures, derived by Rietveld analysis, are: (i) forsterite 83.2 wt%, enstatite 16.7 wt% and cristobalite
220 0.1 wt% for the starting material identified as FoEn, and (ii) magnesite 44.2 wt%, enstatite 39 wt%
221 forsterite 15.3 wt% and cristobalite 1.5 wt%, for the starting material EnMgs.

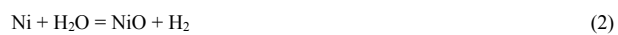
222 To collect fluids and solutes a layer of diamond crystals with grain size of 20 µm was placed
223 between two layers of the starting mineral assemblages (FoEn or EnMgs). All experimental runs were
224 performed at fluid-saturated conditions, with total fluids accounting for ~20 wt%. An additional
225 experimental run was performed at $P = 1$ GPa and $T = 800$ °C employing the starting material FoEn and a
226 single Au capsule to measure the solubility of the assemblage forsterite + enstatite in pure water for
227 comparison with previously published results (Newton and Manning 2002).

228

229 2.2 Experimental strategy

230 As the volatile composition of a graphite-saturated COH fluid is dependent on the redox state of
231 the system, all the experimental runs were performed employing the double capsule technique (Eugster
232 and Skippen 1967) and the nickel-nickel oxide (NNO) buffer to constrain the redox conditions.

233 The inner Au₅₀Pd₅₀ capsule was loaded with the starting materials, FoEn or EnMgs, OAA, ~~H₂O~~Cs-doped
234 ~~water~~, graphite and diamonds (Fig. 1). The outer capsule (Au at $T < 1000$ °C, Pt at $T > 1000$ °C)
235 contained the inner capsule, ~~Ni, NiO~~NNO and H₂O. The NNO buffer fixes the chemical potential of H₂
236 ($f_{H_2}^{NNO}$) in the H₂O-only fluid of the outer capsule. As long as the phases Ni, NiO and H₂O are present
237 the fugacity of H₂ is fixed by the reaction:



239 The Au₅₀Pd₅₀ alloy of the inner capsule is permeable to hydrogen, therefore the chemical potential of H₂
240 is expected to be homogeneous in the inner and in the outer capsules. Since the inner capsule will contain
241 in general a fluid with other COH species (such as CO₂) in addition to H₂O, the oxygen chemical
242 potential in the inner capsule will be lower (Luth 1989) and can be calculated by thermodynamic
243 modeling along with the volatile composition of the graphite saturated COH fluid.

244 The fugacities of oxygen ($f_{O_2}^{NNO}$) and hydrogen ($f_{H_2}^{NNO}$) fixed in the outer capsule by NNO
245 were calculated employing the software package Perple_X (Connolly 1990; <http://www.perplex.ethz.ch/>)
246 and the thermodynamic dataset of Holland and Powell (1998) ~~revised by these authors in 2004~~. The
247 routines “vertex” and “fluids” were used first to calculate the fugacity of hydrogen fixed in the outer
248 capsule by NNO + H₂O (Perple_X equation of state no. 16; H–O HSMRK/MRK hybrid EoS). Then, we
249 calculated the speciation of the COH fluid through the Excel spreadsheet GFluid (Zhang and Duan 2010)
250 with the EoS of Zhang and Duan (2009) and a modified H₂ fugacity coefficient (γ_{H_2}) changing
251 dynamically as a function of $X(O)$, fitted from the EoS of Connolly and Cesare (1993). This model has
252 been proved to reproduce the composition of COH fluids in the pure C–O–H system (Tumiati et al. ~~in~~
253 [review2017](#)). By assuming that f_{H_2} of the COH fluid in the inner capsule is equal to $f_{H_2}^{NNO}$, we were able
254 to calculate the molar fractions of volatiles (H₂O, CO₂, CO, CH₄, H₂ and O₂) at the investigated pressure
255 and temperature conditions. The predicted fluids are mainly composed of H₂O and CO₂, with X_{CO_2} ratios
256 changing as a function of pressure and temperature (Table 1).

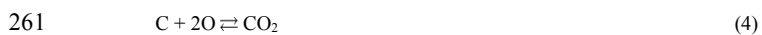
Formattato: Tipo di carattere: Corsivo

Formattato: Pedice

Formattato: Apice

Formattato: Non Evidenziato

257 At $T > 700$ °C, the COH volatile composition is enriched in CO_2 compared to the starting
258 equimolar $\text{H}_2\text{O}-\text{CO}_2$ composition given by OAA and H_2O . Equilibration of the COH fluid is
259 accomplished by these coupled reactions:



262 which can be condensed to the following water- (and graphite-) consuming reaction:

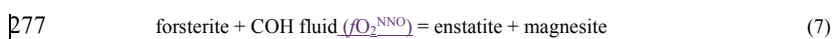


264 The equilibration of the COH fluid at the experimental conditions implies that CO_2 is produced in the
265 inner capsule by oxidation of graphite, a process that requires oxygen, which is taken from the
266 dissociation of water. As a consequence, not only the $X_{\text{H}_2\text{O}}$ [$=\text{H}_2\text{O}/(\text{H}_2\text{O} + \text{CO}_2)$] of the COH fluid, but
267 also the absolute quantity of water decreases in the inner capsule until equilibrium is reached at the
268 experimental P and T conditions.

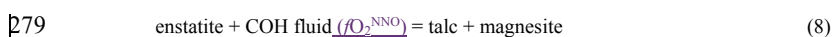
269 A $P-T$ pseudosection for the system MS + COH at $f_{\text{O}_2}^{\text{NNO}}$ conditions was compiled employing
270 the software Perple_X (Connolly 1990). As the composition of the COH fluid is constrained by the
271 oxygen fugacity conditions, ~~but is~~ variable in the $P-T$ field, the $f_{\text{O}_2}^{\text{NNO}}/f_{\text{O}_2}$ conditions ~~retrieved by~~
272 ~~thermodynamic modelling~~ were fitted in equation:

$$273 \quad \ln f_{\text{O}_2} = 10.75 + (-50077 + 0.32196 P) / T \quad (6)$$

274 (P in bar and T in K), ~~which account for the variations in and the~~ COH fluid composition ~~in the $P-T$ field~~
275 ~~is calculated accordingly~~. ~~By fixing $f_{\text{O}_2}^{\text{NNO}}$,~~ ~~the two resulting univariants (black solid lines in Fig. 2) are~~
276 given by the reactions:



278 and



280 On the basis of the predicted stable assemblage in the $P-T$ field we select as starting materials either
281 FoEn or EnMgs (see Supplementary Material).

282

283 2.3 Experimental conditions

284 Experiments were carried out in a rocking piston-cylinder apparatus at pressures from 1.0 to 2.1
285 GPa and temperatures from 700 to 1200 °C. ~~A r~~Rocking piston-cylinder apparatus was employed to

Formattato: Tipo di carattere: Corsivo

Formattato: Pedice

Formattato: Apice

Formattato: Tipo di carattere: Corsivo

286 guarantee the homogeneity of the sample through a rotation of 180° ~~of the entire structure of the piston~~
287 ~~cylinder apparatus~~. The rotation induces Rayleigh-Taylor instabilities, forcing the fluid to migrate and
288 promoting chemical homogenization (Schmidt and Ulmer 2004). During the heating ~~phase stage~~, the
289 piston-cylinder rotated continuously (one turn of 180° every 30 s), then the rotation ~~rate interval~~ was
290 changed to ~~99-100~~ seconds. Experiments were performed for an average run time of 48 h. Quench rates
291 are variable from 25 °C/second to 40 °C/second ~~at higher temperature conditions ($T > 1000$ °C)~~. The
292 assembly consists in NaCl, Pyrex, a graphite heater and graphite disks at the bottom. The capsule was
293 embedded in MgO rods filled with MgO powder. After the experimental run the recovered capsules were
294 cleaned with diamond router bites and rinsed in ~~a diluted~~ HCl solution for 5 hours to eliminate residues of
295 MgO from the capsule.

296

297 3. Analytical technique

298 The solute content in the fluid was measured through the cryogenic laser-ablation ICP-MS
299 (Aerts et al. 2010), ~~a modified version of the technique also known as the~~ “freezing technique” (Kessel et
300 al. 2004), which was applied ~~in this experimental study~~ for the first time on double capsules bearing COII
301 fluids. The recovered experimental capsule was mounted on a freezing stage representing the base of the
302 laser ablation cell, consisting of a stack of two Peltier elements, surrounded by plastic to thermally
303 insulate the elements from the atmosphere (Aerts et al. 2010). The capsule holder is inserted into a copper
304 block in direct contact with the Peltier elements and cooled to $T = -35$ °C. Conventionally, ~~the frozen~~
305 ~~single capsules were can be~~ cut open by hand using a razor blade (Kessel et al. 2004; Aerts et al. 2010);
306 ~~H~~however, this ~~method~~ was hardly possible (and thus poorly controlled) in the present case because of
307 the toughness of ~~the Ni-bearing~~ double capsules. Consequently, ~~controlled~~ capsule cutting was ~~ensured~~
308 ~~via addition of performed using~~ a mechanical cutting device onto the freezing stage (Fig. 3a). This device
309 allows to expose a longitudinal cross-section of the capsule by fastening a screw that pushes a cutter
310 blade mechanically guided through a copper vice holding the capsule (Fig. 3b) while all is kept at -35 °C
311 in ~~a hood box~~ flushed with dry Ar. Once the capsule is opened, the device is removed from the freezing
312 stage together with the upper part of the capsule holder. The upper half of the capsule is inspected with a
313 binocular microscope to help locating the diamond trap, while the lower part, always kept frozen, is

314 covered by the ablation cell top (Fig. 3c) and transferred to the microscope stage for ~~laser-ablation~~
315 ~~LA-~~ ICP-MS measurements.

316 The analyses were performed using a 193 nm ArF GeoLas Pro excimer laser system coupled to
317 an ELAN DRC-e quadrupole mass spectrometer at the University of Bern. We analyzed the diamond trap
318 for ^{24}Mg , ^{25}Mg , ^{26}Mg , ^{29}Si , ^{62}Ni , ^{133}Cs , ^{195}Pt and ^{197}Au , using a 60 μm beam diameter, $\sim 13 \text{ J/cm}^2$ laser
319 fluence and 5 Hz repetition rate. For Mg, all three isotopes were recorded in order to constrain the effect
320 of polyatomic gas interferences ($^{12}\text{C}^{12}\text{C}$, $^{12}\text{C}^{13}\text{C}$, $^{12}\text{C}^{14}\text{N}$) on the final results. At $-35 \text{ }^\circ\text{C}$ set in the freezing
321 stage the CO_2 fraction unmixed from the COH fluid upon quench is not frozen, thus accounting for the
322 low coherence of the trap during laser ablation measurement (and resulting craters were not well defined).
323 Data were acquired in blocks of up to ~ 10 individual sample analyses bracketed by three analysis of the
324 standard NIST SRM610, placed in the ablation chamber with the sample. Background was taken for ~ 50
325 seconds and the sample signal, on the diamond trap or on the solid residue, was collected for ~ 20
326 seconds. LA-ICP-MS data reduction was performed employing the software Sills (Guillong et al. 2008;
327 <http://www.geopetro.ethz.ch/research/orefluids/software>) and in-house spreadsheets to calculate solute
328 concentrations employing rigorous limits of detection filtering (Pettke et al. 2012) for each element and
329 each measurement individually.

330 The cryogenic ~~LA-ICP-MS~~ technique was originally developed to analyze the solute content ~~of~~
331 ~~in systems containing only~~ H_2O ~~as volatile fluid component-only fluids~~. Cesium, introduced in the starting
332 materials, is employed as ~~the an~~ internal standard for data quantification, because it is a highly
333 incompatible element that ~~fractionates-partitions~~ completely into the fluid with the given mineral
334 assemblages. In our experiments, we introduced a known amount of water ~~solution~~-doped with 585 $\mu\text{g/g}$
335 Cs [as $\text{Cs}(\text{OH})_2$]. As the initial Cs/ H_2O ratio ~~was-is~~ fixed, once the Cs concentration in the fluid phase
336 coexisting with minerals at run P and T is known, solute concentrations of the fluid can be calculated
337 (Kessel et al. 2004). However, compared to experiments bearing aqueous fluids coexisting with
338 anhydrous silicates, our double-capsule, COH-bearing experiments are more complex, because (i) there is
339 one fluid phase at run conditions (mostly a $\text{H}_2\text{O} + \text{CO}_2$ mixed fluid, plus solutes), exsolving two fluid
340 phases (liquid H_2O + solutes, and gaseous CO_2) at quench conditions (see Fig. 1) and (ii) the initial
341 Cs/ H_2O is not fixed in our experiments, because the water content in the runs is variable, depending on P ,
342 T and $f\text{O}_2$ conditions. In double capsule arrangements, H_2 is in fact a mobile component that can be added

343 or removed from the system through diffusion in and out of the inner capsule. These conditions imply
 344 that the LA-ICP-MS data on systems bearing COH fluids refer to the aqueous part of fluids only,
 345 assuming that no solutes escape with the carbonic gas species upon capsule opening. Moreover, the latter
 346 point implies the initial Cs concentration cannot be used as an internal standard, unless this value is
 347 corrected to the X_{H_2O} in the fluid at run P and T . To retrieve the amount of solutes in terms of mol/kg_{H₂O}
 348 a correction for the change in total water mass present in the capsule relative to initial water mass loaded
 349 into the capsule is thus required.

350 If H₂O is consumed during fluid re-equilibration at run conditions, Cs concentration in the
 351 residual water increases; if H₂O is produced, Cs concentration decreases. We estimated the corrected Cs
 352 concentration at run P and T using a model, which assumes that fluid equilibration at NNO hydrogen
 353 fugacity condition is governed only by H₂ mobility and no hydration or carbonation reactions involving
 354 minerals occur in the capsule charge. As long as these two assumptions are valid, it is possible to estimate
 355 the amount of Cs in the inner capsule in the following way using a classic dilution equation:

$$356 \quad C_i Cs * V_i H_2O = C_f Cs * V_f H_2O \quad (9)$$

357 where $C_i Cs$ is the initial concentration of Cs in the aqueous solution loaded into the capsule (585
 358 ppm) and $C_f Cs$ is the final concentration of Cs after fluid equilibration at $f_{H_2}^{NNO}$ conditions. $V_i H_2O$ and
 359 $V_f H_2O$ are the initial and final volume of water.

360 The volume of water is proportional to the moles according to:

$$361 \quad V_{H_2O} = n_{H_2O} * V_{mol, H_2O} \quad (10)$$

362 (V_{H_2O} , volume of water; n , number of H₂O moles; V_{mol, H_2O} , molar volume of water).

363 Considering that at fixed pressure and temperature conditions the molar volume of water is
 364 constant we obtain the following dilution equation:

$$365 \quad C_i Cs * n_i H_2O = C_f Cs * n_f H_2O \quad (11)$$

366 where $C_i Cs$ is the initial concentration of Cs in the aqueous solution loaded into the capsule (585 $\mu\text{g/g}$)
 367 and $C_f Cs$ is the final concentration of Cs after fluid equilibration at $f_{H_2}^{NNO}$ conditions. $n_i H_2O$ and $n_f H_2O$
 368 are the initial and final number of H₂O moles.

369 The final Cs concentration will be given by:

$$370 \quad C_f Cs = \frac{C_i Cs * n_i H_2O}{n_f H_2O} \quad (12)$$

Formattato: Normale, Rientro: Prima riga: 1,25 cm

Formattato: Normale, Rientro: Prima riga: 1,25 cm

Formattato: Pedice

371 As $n_{\text{H}_2\text{O}}$ is known, i.e. the initial amount of water charged into the capsule, Eqn. (102) can be solved as
372 long as $n_{\text{H}_2\text{O}}$ is constrained. Solute concentrations in the pure water fraction of the fluid at run P and T
373 can thus be calculated. For one experimental run, performed at 1 GPa and 800 °C, the volatile speciation
374 of the fluid was retrieved experimentally by employing the capsule-piercing QMS technique (Tiraboschi
375 et al. 2016) instead of calculating the amount of H₂O and CO₂ through thermodynamic modeling. The
376 volatile composition consists of CO₂ (84.2 wt.%) and H₂O (15.8 wt.%). Compared to the experimental
377 model employed to quantify the internal standard, the experimental volatile speciation appears to be
378 enriched in CO₂ (see Table 1). The discussion relative to the different volatile speciation is presented
379 elsewhere (Tumiati et al. [in-review2017](#)). However, since the experimental result shows that the amount
380 of H₂O in the inner capsule could be more variable than expected, the solubility of silica and magnesia~~um~~
381 were also calculated by varying the amount of H₂O in the experiments (plus or minus ~~the 50 wt.%;~~
382 available as Supplementary Material). Varying the amount of water does not affect significantly the
383 amount of solutes, which variations are dominated by the analytical error. Consequently, the volatile
384 speciation derived from thermodynamic modeling was employed to retrieve the solubility for all the other
385 experimental runs.

386 For the experimental runs performed in the stability field of magnesite, we employed the EnMgs
387 starting material to minimize the amount of newly formed carbonates. X-ray maps of elements and
388 Principal Component Analysis (PCA) were ~~considered-used~~ to evaluate the relative abundances of solid
389 phases in the experimental runs and estimate the amount of CO₂ consumed to form new magnesite
390 crystals. In fact, the initial amount of water charged in the capsule ($n_{\text{H}_2\text{O}}$) will readjust if part of the
391 initial CO₂ is consumed to form carbonates, as the system is buffered at NNO oxygen fugacity conditions.
392 To maintain the CO₂/H₂O ratio determined by the oxygen fugacity conditions the amount of H₂O has to
393 decrease in the inner capsule. Consequently the experimental runs performed in the magnesite stability
394 field required an additional Cs correction. Capsules were inspected at the electron microscope (JEOL
395 8200 Superprobe, University of Milan) for ~~presence of quench the eventual presence of~~ precipitate
396 ~~magnesites~~ in the diamond layer. Then the capsules were embedded in epoxy and polished, in order to
397 perform ~~wavelength-dispersive X-ray spectroscopy (WDS) electron probe~~ analyses and X-ray elemental
398 maps.

399

400 4. Results

401 In Figure 23, the run products are displayed together with the experimental carbonation curve of
402 forsterite, determined on the basis of textural observations. The X_{CO_2} of the fluid ~~given is shown~~ as gray
403 shaded contours. At the P - T - fO_2 conditions investigated ~~from low to high pressure~~, we ~~first~~ observed
404 ~~three mineral~~ the assemblage: (i) forsterite + enstatite (fo + en) ~~assemblage~~, then: (ii) talc + magnesite (tc
405 + mgs); (iii) ~~then~~ enstatite + magnesite (en + mgs). The majority of the experimental runs that started
406 with the FoEn mix gave the same run products of forsterite + enstatite after the quench, with the
407 exception of two experimental runs: (i) 1.5 GPa and 900 °C and (ii) 2 GPa and 1200 °C. At 1.5 GPa and
408 900 °C we observed newly formed magnesite from the forsterite + enstatite assemblage (Fig. 4a). At 2
409 GPa and 1200 °C the experimental run presents a sponge-like texture consisting of SiO_2 (Fig. 4b) with
410 small dispersed enstatite crystals. No forsterite crystals were identified at these conditions; however, it
411 has to be noted that the capsule was severely damaged during the cutting procedure for LA analyses. The
412 experimental runs performed employing the EnMgs starting material at low- T conditions yielded the
413 assemblage enstatite + talc + residual magnesite, and forsterite coronas were observed surrounding
414 magnesite crystals at 1.2 GPa and 800 °C (Fig. 4c).

415 The solubility results expressed as mol/kg H_2O are reported in Table 2, together with the total
416 amounts of solutes in wt.% and the calculated Cs concentrations (in $\mu g \cdot g^{-1}$) prevailing at run conditions
417 in the pure water. No solubility data were obtained above 2 GPa and 1100 °C and at 1.5 GPa and 1100
418 °C, as the diamond trap was not completely preserved at these conditions (Fig. 4b and 4d). Moreover,
419 solubilities were not retrieved at 1.5 GPa and 700 °C and 1.2 GPa and 800 °C due to the lack of
420 equilibrium between solid phases (i.e., magnesite in the talc + enstatite assemblage and forsterite coronas
421 on magnesite relics). In all experimental runs the NNO buffer assemblage was preserved after the quench.
422 Graphite was also preserved below 2 GPa and 1200 °C.

423 Concerning analytical errors, Kessel et al. (2004) determined an uncertainty in the amount of
424 H_2O in the fluid, derived from Cs analysis, ranging from 0.7 to 2.5%, which was similar (or smaller) than
425 the standard deviation of their data. In our case, for each experiment, we reported the standard deviation,
426 as our values are higher compared to the maximum uncertainty (2.5%) determined by Kessel et al.
427 (2004). However, if only one laser-ablation shot is available (experimental runs CZ6, CZ5 and CZ9) we
428 consider a minimum analytical error corresponding to that given by Kessel et al. (2004).

Formattato: Rientro: Prima riga: 1,25 cm

429

430 4.1 Forsterite + enstatite assemblage

431 The SiO₂ contents reported as weight percentage in the water fraction of the fluid equilibrated ~~in~~
432 ~~the aqueous fraction of the COH fluid deriving from the equilibration~~ with forsterite and enstatite (Table
433 2) increases with pressure and temperature from 0.85 ± 0.15 mol/kg_{H₂O} at 1 GPa and 700 °C to $4.21 \pm$
434 0.04 mol/kg_{H₂O} at 1 GPa and 1100 °C and 4.60 ± 0.37 mol/kg_{H₂O} at 2 GPa and 1100 °C (Fig. 5a). The
435 MgO content also rises with *T*, from 0.67 ± 0.06 mol/kg_{H₂O} at 1 GPa and 700 °C to 6.90 ± 0.07 mol/kg_{H₂O}
436 at 1 GPa and 1100 °C; while from 1 to 2 GPa at 1100 °C we observe identical *m*MgO values within errors
437 (6.90 ± 0.04 mol/kg_{H₂O} at 1 GPa; 6.12 ± 0.99 mol/kg_{H₂O} at 2 GPa) (Fig. 5b).

438 The solubility of forsterite + enstatite in COH fluids was compared with the solubility of the
439 same assemblage in pure water, by performing a dissolution experiment at *P* = 1 GPa and *T* = 800 °C
440 (white dots in Fig. 5a). At these conditions, SiO₂ dissolved in pure water (0.22 ± 0.06 mol/kg_{H₂O}) is much
441 lower than SiO₂ dissolved in the COH fluid (1.24 ± 0.19 mol/kg_{H₂O}). In a similar way also the MgO
442 content from forsterite and enstatite dissolution in the COH fluid is higher compared to dissolution in ~~the~~
443 ~~H₂O-only-system~~: from 0.28 ± 0.04 mol/kg_{H₂O} in H₂O to 1.08 ± 0.10 mol/kg_{H₂O} in the MS + COH system
444 (Fig. 5b).

445

446 4.2 Enstatite + magnesite assemblage

447 Two experimental runs were performed above the forsterite carbonation reaction (see Fig. 3).
448 For these experiments the amount of SiO₂ and MgO in the aqueous fraction of the COH fluid was
449 retrieved considering that a part of the initial CO₂ in the inner capsule was consumed to produce
450 carbonates. The amount of SiO₂ at 1.5 GPa from 800 to 900 °C (Table 2) is similar within analytical error
451 (0.41 ± 0.02 mol/kg_{H₂O} at 800 °C; 0.53 ± 0.23 mol/kg_{H₂O} at 900 °C; Fig. 5a), while the *m*MgO tends to
452 increase with temperature from 0.47 ± 0.09 mol/kg_{H₂O} at 800 °C to 0.73 ± 0.29 mol/kg_{H₂O} (within the
453 stated uncertainties; Fig. 5b). Compared to the forsterite + enstatite assemblage, the SiO₂ concentration in
454 the fluid coexisting with enstatite + magnesite is significantly lower, suggesting a lower solubility of
455 enstatite in the COH fluid compared to forsterite. The MgO content is slightly lower compared to the
456 ~~fluid in equilibrium with forsterite and~~ enstatite ~~assemblage~~, however we also have to consider that the

457 pressure conditions are different (1.5 GPa for en + mgs; 1 GPa for fo + en) and the Mg could derive from
458 either magnesite or enstatite, or from a combined effect.

459

460 5. Discussion

461 5.1 Comparison with previous solubility studies

462 In this experimental study, we provide for the first time solubility measurements of forsterite,
463 enstatite and magnesite dissolution in a mixed H₂O–CO₂ fluid in equilibrium with graphite. To validate
464 our approach we also performed an experimental run in the system MgO–SiO₂–H₂O, to compare results
465 of our analytical technique with those obtained in previous studies on mineral solubility. Our
466 experimental data relative to the dissolved SiO₂ in an aqueous fluid coexisting with forsterite and enstatite
467 at 1 GPa and 800 °C ($m_{\text{SiO}_2} = 0.22 \text{ mol/kg}_{\text{H}_2\text{O}}$) is within error identical within uncertainties with the
468 amount of SiO₂ determined by Newton and Manning (2002) ($m_{\text{SiO}_2} = 0.21 \text{ mol/kg}_{\text{H}_2\text{O}}$) considering
469 similar starting materials and run time. Our experimental data fit quite well also with other literature data
470 (Nakamura and Kushiro 1974; Manning and Boettcher 1994; Zhang and Frantz 2000; Newton and
471 Manning 2002) on SiO₂ solubility in the same system (white dot in Fig. 6a, open symbols), considering
472 the differences in starting materials and technique employed demonstrating that different experimental
473 strategies yield comparable results.

474 Regarding the amount of MgO dissolved in an aqueous fluid with forsterite and
475 enstatite is concerned, there are to date no published experimental data available to date for the P – T
476 conditions of 1 GPa and 800 °C investigated here. Extrapolation of MgO solubility derived from the
477 dissolution of forsterite and enstatite in pure water from data obtained at $P = 1$ – 2 GPa and $T = 900$ – 1200
478 °C reported in Zhang and Frantz (2000) suggests a solubility below 0.17 mol/kg for our experimental
479 conditions. Our measured fluid $m_{\text{MgO}} = 0.28 \text{ mol/kg}_{\text{H}_2\text{O}}$ (Fig. 6b) is higher. However, because our value
480 represents the first experimental direct measurement at moderately high-pressure of dissolved MgO in the
481 MgO–SiO₂–H₂O system, this discrepancy cannot be evaluated further.

482

483 5.2 Dissolution of forsterite, magnesite and enstatite in COH fluids and comparisons with 484 dissolution in H₂O-only systems

485 Compared with the solubility in the MgO–SiO₂–H₂O system, both the amounts of SiO₂ and MgO
486 dissolved in the aqueous fraction of a COH fluid from forsterite + enstatite are higher (Fig. 6). This result
487 suggests that, in contrast to what is observed for instance in the SiO₂–H₂O–CO₂ system (Newton and
488 Manning 2000), in the MS-COH system the CO₂ component of the COH fluid does not act merely as an
489 inert diluent, i.e. lowering the amounts of solutes dissolved in the fluid. Instead, carbon dioxide seems to
490 promote the dissolution of Mg-bearing silicates, favoring the formation of complexes involving Mg and
491 C, as suggested by the higher MgO content in the aqueous fraction of COH fluid compared to the MgO
492 dissolved in a H₂O-only fluid at the same experimental conditions ($P = 1$ GPa and $T = 800$ °C). Similarly,
493 as the amount of SiO₂ is also higher compared to dissolution in H₂O-only fluids, the results suggest the
494 formation of complexes potentially involving Mg, C and Si, in addition to the solutes generated by the
495 effect of the aqueous component of the fluid (e.g. silica monomers and dimers [as suggested by following](#)
496 [Newton and Manning 2002](#)). [However, The](#) presence of Si-C complexes has not previously detected in
497 the system SiO₂–H₂O–CO₂, where the main dissolved species was thought to be a neutral dihydrate of
498 silica with one to three attached (solvated) H₂O molecules (Newton and Manning 2000). [However, it](#)
499 should be noted that the [latter-cited](#) experiments did not involve graphite.

500 There are two possible options to interpret the increase in dissolved SiO₂ in the MS-COH
501 system: (i) the generation of Mg-Si-C complexes, and (ii) the production of a SiO₂ residue due to the
502 formation of Mg-C solutes from forsterite and enstatite, which is highly soluble in H₂O (Manning 1994).
503 In this experimental study, the dissolution process has been quantified in terms of absolute major element
504 solubilities in the fluid, therefore information on the speciation can only be gained indirectly, through
505 thermodynamic modeling (see Section 5.3). However, the formation of SiO₂ and Mg-C solutes has been
506 directly observed in the experimental runs where the solubility data were not available ($P > 2$ GPa and T
507 > 1100 °C), as the diamond trap was no longer preserved. In these runs the fluid was not completely
508 ablated during LA-ICP-MS measurement, therefore it was possible to [visualise-characterize](#) precipitates
509 by [backscattered electron \(BSE\)](#) imaging of unpolished and polished samples. At 2.1 GPa and 1100 °C
510 precipitates appear as SiO₂ droplets (Fig. 7a) and as vesiculated aggregate or acicular Mg-C solutes,
511 probably hydrated (Fig 7b). WDS analyses show detectable Cs quantity (up to 0.07 wt.%), while for other
512 solid phases Cs was below detection limit, confirming an origin as fluid quench precipitate. However, we
513 note that in this experimental run, only few diamonds were retrieved. We suggest that diamond

514 dissolution could have occurred at the experimental conditions. In fact, Fedortchouk et al. (2007)
515 observed that after 35 hours at $P = 1$ GPa and $T = 1350$ °C a diamond of 5 mm loses nearly 40 wt.% of its
516 initial weight at NNO oxygen /H₂ conditions. Considering that the diamonds employed in our studies are
517 significant smaller (20 µm) while the experimental pressure is higher ($P = 2$ –2.1 GPa) dissolution seems
518 to be the process most plausible for the lack of diamonds, at least at the highest temperature conditions.

519 At 2 GPa and 1200 °C forsterite, diamonds and graphite were completely dissolved in a silica-
520 rich vesiculated glass with few enstatite crystals dispersed. The observed texture is extremely similar to
521 an experimental run performed by Cruz and Manning (2015) in the SiO₂–H₂O–NaCl system at 1.5 GPa
522 and 1100 °C. The authors suggested that a similar feature indicates the presence of two distinct fluids, one
523 hydrous Si-rich fluid and the other saline and relatively Si poor. In our experimental runs the relatively Si
524 poor fluid could be constituted by Mg–C complexes, as shown in Figure 7a. However, it remains unclear
525 why in this experimental run the Mg-bearing fluid was not identified. Moreover, the presence of a
526 miscibility gap seems unlikely in a NaCl-free system and could result simply from the quench process.

527 In Figure 8, solubilities of silica and magnesite are plotted versus the X_{CO_2} of the coexisting
528 COH fluid. In both cases we observe an increase with temperature and X_{CO_2} . On the other hand, the
529 behavior of SiO₂ and MgO is different when it comes to increasing pressure: while the SiO₂ content
530 slightly increase (Fig. 8a), MgO shows higher values at lower pressure and high temperature conditions
531 ($P = 1$ GPa; $T = 1100$ °C), where the COH fluid is mainly composed by CO₂ ($X_{CO_2} = 0.85$) (Fig. 8b). At
532 high temperature conditions CO₂ favors the formation of Mg–C complexes, while H₂O, present in
533 significantly minor quantity, appear to dissolve less SiO₂. With increasing pressure the X_{CO_2} lowers,
534 consequently the effect of CO₂ is weakening, while the aqueous component becomes more effective in
535 dissolving the SiO₂ residue.

536 The amount of solutes derived from the dissolution ~~in a COH fluid~~ of the assemblage magnesite
537 + enstatite ~~in a COH fluid~~ can be compared to the experimental data from Caciagli and Manning (2003)
538 relative to simple calcite dissolution in H₂O. The dissolved cations in this case are Mg and Si instead of
539 Ca, and the fluid composition is COH fluid instead of pure H₂O. Solute amounts for Mg and Ca are
540 similar and in agreement with literature data (Fig. 9), suggesting similar solubilities for CaCO₃ and
541 MgCO₃ at the PT conditions investigated here, irrespective of the more complex chemistry of our system.
542 As thermodynamic models indicate that pure magnesite is slightly soluble in H₂O at 10 GPa (Pan et al.

Formattato: Pedice

Formattato: Pedice

543 2013) and has a lower solubility compared to calcite over a significant pressure range (1 to 10 GPa). This
544 comparison shows that either (i) the addition of CO₂ to an aqueous fluid enhances magnesite dissolution
545 compared to ~~a~~-H₂O-only, or (ii) that solvation of Mg in our experimental system involves Mg-Si species,
546 or both. Concerning possibility (i) we observe that our experimental amount of SiO₂ dissolved from
547 enstatite is quite similar to that in ~~a~~ H₂O-only fluid (0.41 mol_{SiO₂}/kg_{H₂O} in COH fluid at 1.5 GPa ~~and~~ 800
548 °C versus 0.42 mol_{SiO₂}/kg_{H₂O} at 1 GPa and 850 °C, Newton and Manning 2002). And our SiO₂ solubilities
549 at 1.5 GPa and 900 °C (0.53 mol/kg_{H₂O}) are similar to those obtained for pure water coexisting with
550 enstatite + forsterite at 1.4 GPa and 900 °C (0.51–0.52 mol/kg_{H₂O}; Newton and Manning 2002). SiO₂
551 dissolution thus seems to be governed by the H₂O component, and no positive or negative effect caused
552 by CO₂ addition to the fluid can be discerned. Because the molalities of dissolved Si and Mg are equal
553 within uncertainties, dissolution of a magnesite component is not indicated, which is consistent with the
554 very low Mg solubility reported by Pan et al. (2013).

555

556 5.3 Theoretical solute speciation modeling

557 In order to ~~gain some insight into~~characterize the possible aqueous species relevant to ~~the our~~
558 experimental system ~~investigated~~, we employed a thermodynamic model that, in addition to neutral COH
559 species, also takes into account Mg and Si-bearing dissolved species. We performed calculations using
560 the aqueous speciation-solubility code EQ3 (Wolery 1992) adapted to include equilibrium constants
561 calculated with the Deep Earth Water (DEW) model (Faq et al. 2014; Sverjensky et al. 2014). We
562 focused on the solubility measurements at 800 °C and 1.0 GPa, as results were available for the solubility
563 of Mg and Si in the MS-H system as well as the MS-COH system. The two sets of Mg and Si solubility
564 data enabled characterization of a Mg-OH complex and a Mg-Si-C complex.

565 For the ~~MSH~~system ~~MS-H~~, silica concentrations predicted using the silica monomer and dimer
566 in the DEW model agreed, as expected, with the experimentally measured values. However, matching the
567 experimental Mg concentration required an Mg(OH)₂ complex in addition to the predicted value for
568 Mg(OH)⁺. Trial and error regressions of the experimental data for the MS-H and the MS-COH systems
569 indicated that Mg(OH)⁺ could not account for the measured Mg concentrations in both systems. Instead,
570 the data for the MS-H system was used to retrieve the equilibrium constant for the second Mg(OH)₂
571 complex given by the equilibrium

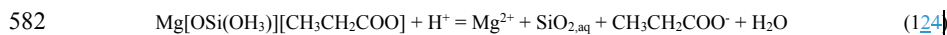
Formattato: Evidenziato

Formattato: Evidenziato



573 as in Table 3.

574 In the system MS-COH, the model Mg-solubilities using the new Mg-OH complexes were still
575 too low, indicating the likely need for additional Mg-bearing complex. Furthermore, the predicted Si-
576 solubility based solely on the monomer and dimer was also way too low because it remained the same as
577 for the C-free system (Table 3). Trial and error regressions using various species such as MgHCO_3^+ ,
578 MgCO_3 , MgHSiO_3^+ , and MgSiO_3 failed to adequately describe the experimental data for the MS-COH
579 system given what was already known about the stabilities of these complexes. Instead, the data for the
580 MS-COH system was used to retrieve the equilibrium constant for a complex involving Mg, Si, and C
581 according to the equilibrium



583 as in Table 3. This complex, which involves carbon, results in the solubility of Mg and Si $f\text{O}_2$ dependent.
584 Propionate involves reduced C. Therefore, calculated solubilities involving Eqn. (124) increase at lower
585 $f\text{O}_2$ values and decrease at higher $f\text{O}_2$ values. Eqn. (124) is only important for reducing systems. It should
586 not be significant at all in COH fluids from all previous studies of Mg-silicate solubilities or stabilities
587 that have focused on oxidizing conditions without graphite. Consequently, Eqn. (124) provides an
588 explanation for the distinctive enhanced solubilities of Mg and Si measured in the present study, which
589 does involve graphite, and, presumably, aqueous species involving reduced carbon. Volatile reduced C-
590 species have in fact been detected in chemical analyses of the volatiles dissolved in the MS-COH system
591 with graphite (Tumiati et al. [in-review2017](#)), as well as implied by model calculations of the COH fluid
592 compositions (Table 1).

593 A more complete analysis of the potential importance of Eqn. (124) over a wide range of
594 temperatures and pressures is hampered by the lack of experimental Mg-solubility data in the MS-H
595 system, which is needed for quantification of Eqn. (113). Consequently, a full equation of state
596 characterization of the standard partial molal properties of the Mg-Si-C-complex must await the
597 development of several estimation schemes for predicting the properties of the Mg-OH complex in Eqn.
598 (113). This will be the subject of a future study.

599

600 **5.4 Forsterite carbonation curve**

601 Although the experiments performed were aimed to measure fluid composition and were not
602 reversed, we reported in Fig. 2 the forsterite carbonation reaction. The reaction shows a weak pressure
603 dependency and occurs at higher pressure compared to the one determined by Koziol and Newton (1998)
604 in the MgO–SiO₂–CO₂ system. The shift toward higher pressures is predicted also by the calculated
605 reaction through a thermodynamic model and is probably caused by the presence of H₂O in the
606 investigated experimental system. With increasing temperatures and molar fraction of CO₂ the reaction
607 approaches that of Koziol and Newton (1998) as the composition of the fluid becomes more CO₂ rich.

608

609 5.5. Implications for metasomatic processes

610 Several authors investigated the MSH system as a simplified model for melting and solubility in
611 hydrated peridotites (e.g., Kushiro et al. 1968; Ryabchikov et al. 1982; Inoue 1994; Luth 1995; Zhang and
612 Frantz 2000; Stalder et al. 2001; Mibe et al. 2002; Hack et al. 2007). Available experimental data on
613 mineral solubility in the MSH system indicates that at low-pressure conditions (< 3 GPa) the amount of
614 dissolved SiO₂ in the aqueous fluid is significantly higher compared to MgO (e.g., Zhang and Frantz
615 2000; Newton and Manning 2002). At these conditions, an aqueous fluid, migrating upward through the
616 upper mantle, dissolves up to the 20 wt.% of silica, leaving a SiO₂-depleted mantle and a relatively SiO₂-
617 enriched crust (Nakamura and Kushiro 1974). This process results in the formation of enstatite relative to
618 forsterite, as the Mg/Si ratio is significantly lower than unity. However, the Mg/Si ratio derives from
619 experimental data limited to SiO₂, as no measures of MgO solubility in aqueous fluid are available at low-
620 pressure conditions. Our experimental study presents for the first time, the amount of both SiO₂ and MgO
621 dissolved in an aqueous fluid in equilibrium with forsterite and enstatite (MSH system) and consequently
622 provides the first experimentally based Mg/Si ratio. At 1 GPa and 800 °C the aqueous fluid shows a
623 significantly higher Mg/Si ratio (= 1.27) than previously reported in literature.

624 In Figure 10 a ~~thermodynamic model~~- X isobaric pseudosection is presented to show the effect
625 of variable Mg/Si ratios in the fluids reacting with ~~fa~~ forsterite, being $Mg/Si = 0$ at $X = 0$, and $Mg/Si =$
626 $1/2$ at $X = 1$. Assuming a complete reaction between 25 wt % fluid and 75 wt % forsterite, fluids with a
627 Mg/Si ratios < 2 will modify the system bulk compositions, so that enstatite may form. In the MSH
628 system the amount of enstatite produced by this fluid is approximately + 10 mol% (open symbol in Fig.
629 10). In the MS + COH system the Mg/Si ratio is lower compared to the MSH system (filled symbols in

Formattato: Tipo di carattere: Grassetto

Formattato: Rientro: Prima riga: 1,25 cm

Formattato: Tipo di carattere: Corsivo

Formattato: Tipo di carattere: Corsivo

Formattato: Tipo di carattere: Corsivo

Formattato: Tipo di carattere: Corsivo

630 Fig. 10) and increases with temperature. At low- T conditions the amount of enstatite produced by the
631 reaction would be higher ($\sim + 17$ mol%) compared to high- T conditions, where the amount of
632 orthopyroxene produced will be less than 5 mol%. The calculated amount of fluid, expressed as $\text{g}_{\text{H}_2\text{O}}/\text{mol}$
633 forsterite, to complete the reaction varies from 197 in the MS + COH system to 602 in the MSH system at
634 1 GPa and 800 °C. Therefore, in the MS + COH system lowers amounts of fluid are required to
635 metasomatize the forsterite compared to the MSH system, where a significant higher quantity of water is
636 needed. Moreover, with increasing temperature the amount of fluid employed to complete the reaction
637 lowers, reaching 27 $\text{g}_{\text{H}_2\text{O}}/\text{mol}$ forsterite at 1 GPa and 1100 °C.

Formattato: Pedice

638 Our experimental data shows that at low temperature conditions a CO_2 -bearing fluid could
639 produce higher amount of enstatite compared to an aqueous fluid, while at high temperature conditions (T
640 > 1000 °C) the fluid seems to be less effective in metasomatize the surrounding forsterite. In a mantle
641 wedge flushed by H_2O and CO_2 in presence of graphite (Galvez et al. 2013), where subsolidus conditions
642 prevail, the formation of enstatite would be favored compared to a system where the only volatile species
643 is H_2O . On the other hand, higher temperature conditions will favor the migration of C-, Mg- and Si-
644 bearing fluids to shallowest level in the upper mantle, as the fluid is less reactive with the surrounding
645 forsterite.

Formattato: Pedice

Formattato: Rientro: Prima riga: 1,25 cm, Nessun controllo righe isolate, Non regolare lo spazio tra testo asiatico e in alfabeto latino, Non regolare lo spazio tra testo asiatico e caratteri numerici

Formattato: Tipo di carattere: Corsivo

646

647 6. Conclusions

648 In this experimental work we present the first measurements of dissolved SiO_2 and MgO in
649 graphite-saturated COH fluids from two different assemblages, forsterite + enstatite and magnesite +
650 enstatite. We employed the cryogenic LA-ICP-MS technique on double capsule assemblages to quantify
651 SiO_2 and MgO solubility in the aqueous fraction of COH fluids buffered at Ni-NiO- H_2O . The presence
652 of CO_2 increases the solubility of forsterite and enstatite compared to ~~systems containing only H_2O only~~
653 ~~as volatile component fluid~~. Moreover, magnesite solubility in a COH fluid is similar to that of calcite in
654 pure H_2O . Our results indicate that in a Mg-bearing system CO_2 does not act merely as an inert diluent,
655 by lowering the solubility of solid phases. On the contrary, CO_2 favors the formation of Mg-Si-C
656 complexes, leading to a graphite-saturated COH fluid containing significant amounts of dissolved
657 reduced carbon species. Our experimental study highlights the importance of COH fluids in transporting
658 Mg, Si, and C at subsolidus conditions. At high temperature conditions these fluids seem to interact

Formattato: Rientro: Prima riga: 1,25 cm

659 [poorly with the surrounding peridotite and could represent an effective way to mobilize C-bearing species](#)
660 [to shallowest level in the mantle, along with diapirism of slab rocks \(Marschall and Schumacher 2012;](#)
661 [Tumiati et al. 2013\) and melt generation \(Poli 2015\).](#)

662 ~~Overall~~ [From an analytical point of view](#), the cryogenic LA-ICP-MS technique, coupled with
663 other techniques to characterize the volatile speciation of the fluid (e.g., Tiraboschi et al. 2016) represent
664 a significant improvement towards a comprehensive characterization of fluids, in terms of volatile
665 speciation and dissolved solute species.

666

667 **Acknowledgments**

668 [Authors are indebted to A. Risplendente for the assistance at scanning electron microscope and](#)
669 [electron microprobe. Editorial handling by M.W. Schmidt and reviews from two anonymous reviewers](#)
670 [significantly improved the manuscript.](#) Funding was provided by the Italian [Ministry of Education,](#)
671 [University and Research \(MIUR\)](#) program PRIN2012R33ECR. C.T., [S.T.](#), D.S. and S.P. acknowledge
672 supports from the Deep Carbon Observatory (DCO).

673

674 **References**

- 675 Aerts M, Hack AC, Reusser E, Ulmer P (2010) Assessment of the diamond-trap method for studying
676 high-pressure fluids and melts and an improved freezing stage design for laser ablation ICP-MS
677 analysis. *Am Mineral* 95:1523–1526.
- 678 Anderson GM, Burnham CW (1965) The solubility of quartz in super-critical water. *Am. J. Sci.* 263:494–
679 511.
- 680 Aranovich LY, Newton RC (1999) Experimental determination of CO₂-H₂O activity-composition
681 relations at 600–1000 °C and 6–14 kbar by reversed decarbonation and dehydration reactions. *Am*
682 *Mineral* 84:1319–1332.
- 683 Baker MB, Stolper EM (1994) Determining the composition of high-pressure mantle melts using
684 diamond aggregates. *Geochim Cosmochim Acta* 58:2811–2827. doi: 10.1016/0016-
685 7037(94)90116-3
- 686 Caciagli NC, Manning CE (2003) The solubility of calcite in water at 6-16 kbar and 500-800 °C. *Contrib*
687 *to Mineral Petrol* 146:275–285. doi: 10.1007/s00410-003-0501-y
- 688 Connolly JA–D (1990) Multivariable phase-diagrams - an algorithm based on generalized
689 thermodynamics. *Am. J. Sci.* 290:666–718.
- 690 Connolly JA–D, Cesare B (1993) C-O-H-S [Fluid c](#)Composition and [o](#)Oxygen [f](#)Fugacity in [g](#)Graphitic
691 [m](#)Metapelites. *J. Metamorph. Geol.* 11:379–388.

Formattato: Rientro: Prima riga: 1,25 cm

Formattato: Pedice

Formattato: Pedice

692 Cruz MF, Manning CE (2015) Experimental determination of quartz solubility and melting in the system
693 $\text{SiO}_2\text{-H}_2\text{O-NaCl}$ at 15–20 kbar and 900–1100 °C: implications for silica polymerization and the
694 formation of supercritical fluids. *Contrib to Mineral Petrol*: doi: 10.1007/s00410-015-1187-7

695 Dolejs D, Manning CE (2010) Thermodynamic model for mineral solubility in aqueous fluids: theory,
696 calibration and application to model fluid-flow systems. *Geofluids* 10:20–40. doi: 10.1111/j.1468-
697 8123.2010.00282.x

698 Eugster HP, Skippen GB (1967) Igneous and metamorphic reactions involving gas equilibria. *Res*
699 *geochemistry* 2:492–520.

700 Facq S, Daniel I, Montagnac G, [Cardon H, Sverjensky Det al](#) (2014) In situ Raman study and
701 thermodynamic model of aqueous carbonate speciation in equilibrium with aragonite under
702 subduction zone conditions. *Geochim Cosmochim Acta* 132:375–390. doi:
703 10.1016/j.gca.2014.01.030

704 Fedortchouk Y, Canil D, Semenets E (2007) Mechanisms of diamond oxidation and their bearing on the
705 fluid composition in kimberlite magmas. *Am Mineral* 92:1200–1212. doi: 10.2138/am.2007.2416

706 Fein JB, Walther J-V (1989) Calcite solubility and speciation in supercritical NaCl-HCl aqueous fluids.
707 *Contrib to Mineral Petrol* 103:317–324. doi: 10.1007/BF00402918

708 [Galvez ME, Beyssac O, Martinez I, Benzerara K, Chaduteau C, Malvoisin B, Malavieille J \(2013\)](#)
709 [Graphite formation by carbonate reduction during subduction. *Nat Geosci* 6:473–477.](#)
710 [doi:10.1038/ngeo1827](#)

711 Guillong M, Meier DL, Allan MM, [Heinrich CA, Yardley BW et al](#) (2008) Appendix A6: SILLS: A
712 MATLAB-based program for the reduction of laser ablation ICP-MS data of homogeneous
713 materials and inclusions. *Mineral Assoc Canada Short Course Ser* 40:328–333.

714 [Hack AC, Thompson AB, Aerts M \(2007\) Phase relations involving hydrous silicate melts, aqueous](#)
715 [fluids, and minerals. *Rev Mineral Geochem* 65: 129–185. doi: 10.2138/rmg.2007.65.5](#)

716 Holland TJB, Powell R (1998) An internally consistent thermodynamic data set for phases of petrological
717 interest. *J Metamorph Geol* 16:309–343. doi: 10.1111/j.1525-1314.1998.00140.x

718 [Inoue T \(1994\) Effect of water on melting phase relations and melt composition in the system \$\text{Mg}_2\text{SiO}_4\text{-}\$](#)
719 [\$\text{MgSiO}_3\text{-H}_2\text{O}\$ up to 15 GPa. *Phys Earth Planet Int* 85:237–263.](#)

720 Kawamoto T, Matsukage KN, Mibe K, [Isshiki M, Nishimura K, Ishimatsu N, Ono S et al](#) (2004a) Mg/Si
721 ratios of aqueous fluids coexisting with forsterite and enstatite based on the phase relations in the
722 $\text{Mg}_2\text{SiO}_4\text{-SiO}_2\text{-H}_2\text{O}$ system. *Am Mineral* 89:1433–1437.

723 Kawamoto T, Ochiai S, Kagi H (2004b) Changes in the structure of water deduced from the pressure
724 dependence of the Raman OH frequency. *J Chem Phys* 120:5867–5870. doi: 10.1063/1.1689639

725 [Kessel R, Ulmer P, Pettke T, Schmidt MW, Thompson AB et al \(2004\) A novel approach to determine](#)
726 [high-pressure high-temperature fluid and melt compositions using diamond-trap experiments. *Am*](#)
727 [Mineral 89:1078–1086.](#)

728 Kessel R, Schmidt MW, Ulmer P, Pettke T (2005a) Trace element signature of subduction-zone fluids,
729 melts and supercritical liquids at 120–180 km depth. *Nature* 437:724–727. doi:
730 10.1038/nature03971

Formattato: Pedice

Formattato: Pedice

Formattato: Pedice

Formattato: Pedice

Formattato: Pedice

Formattato: Pedice

Formattato: Pedice

Formattato: Pedice

Formattato: Pedice

Formattato: Pedice

731 ~~Kessel R, Ulmer P, Pettko T, et al (2004) A novel approach to determine high-pressure high-temperature~~
732 ~~fluid and melt compositions using diamond trap experiments. Am Mineral 89:1078–1086.~~
733 Kessel R, Ulmer P, Pettko T, [Schmidt MW, Thompson AB et al](#) (2005b) The water-basalt system at 4 to 6
734 GPa: Phase relations and second critical endpoint in a K-free eclogite at 700 to 1400 °C. Earth
735 Planet Sci Lett 237:873–892. doi: 10.1016/j.epsl.2005.06.018
736 Koziol AM, Newton RC (1998) Experimental determination of the reaction: Magnesite + enstatite =
737 forsterite + CO₂ in the ranges 6-25 kbar and 700-1100 °C. Am Mineral 83:213–219.
738 [Kushiro I \(1969\) System forsterite-diopside-silica with and without water at high pressures. Am J Sci](#)
739 [267A:269–294.](#)
740 Luth RW (1989) Natural versus experimental control of oxidation state : Effects on the composition and
741 speciation of C-O-H fluids. Am Mineral 74:50–57.
742 [Luth RW \(1995\) Is phase A relevant to the Earth's mantle? Geochim Cosmochim Acta 59:679–682.](#)
743 [doi:10.1016/0016-7037\(95\)00319-U](#)
744 Manning CE (1994) The solubility of quartz in H₂O in the lower crust and upper mantle. Geochim
745 Cosmochim Acta 58:4831–4839. doi: 10.1016/0016-7037(94)90214-3
746 Manning CE, Boettcher SL (1994) Rapid-quench hydrothermal experiments at mantle pressures and
747 temperatures. Am Mineral 79:1153–1158.
748 [Marschall HR, Schumacher JC \(2012\) Arc magmas sourced from mélange diapirs in subduction zones.](#)
749 [Nat Geosci 5. 862–867. doi: 10.1038/ngeo1634](#)
750 Melekhova E, Schmidt MW, Ulmer P, Pettko T (2007) The composition of liquids coexisting with dense
751 hydrous magnesium silicates at 11-13.5 GPa and the endpoints of the solidi in the MgO-SiO₂-H₂O
752 system. Geochim Cosmochim Acta 71:3348–3360. doi: 10.1016/j.gca.2007.03.034
753 [Mibe K, Fujii T, Yasuda A \(2002\) Composition of aqueous fluid coexisting with mantle minerals at high](#)
754 [pressure and its bearing on the differentiation of the Earth's mantle. Geochim Cosmochim Acta 66:](#)
755 [2273–2285. doi:10.1016/S0016-7037\(02\)00856-6](#)
756 Nakamura Y, Kushiro I (1974) Composition of the gas phase in Mg₂SiO₄-SiO₂-H₂O at 15 kbar. Carnegie
757 Inst Washingt Yearb 73:255–258.
758 [Newton RC, Manning CE \(2000\) Quartz solubility in H₂O-NaCl and H₂O-CO₂ solutions at deep crust-](#)
759 [upper mantle pressures and temperatures: 2-15 kbar and 500-900°C. Geochim Cosmochim Acta](#)
760 [64:2993–3005. doi: 10.1016/S0016-7037\(00\)00402-6](#)
761 Newton RC, Manning CE (2002) Solubility of enstatite + forsterite in H₂O at deep crust/upper mantle
762 conditions: 4 to 15 kbar and 700 to 900°C. Geochim Cosmochim Acta 66:4165–4176. doi:
763 10.1016/S0016-7037(02)00998-5
764 ~~Newton RC, Manning CE (2000) Quartz solubility in H₂O-NaCl and H₂O-CO₂ solutions at deep crust-~~
765 ~~upper mantle pressures and temperatures: 2-15 kbar and 500-900°C. Geochim Cosmochim Acta~~
766 ~~64:2993–3005. doi: 10.1016/S0016-7037(00)00402-6~~
767 Newton RC, Manning CE (2009) Hydration state and activity of aqueous silica in H₂O-CO₂ fluids at high
768 pressure and temperature. Am Mineral 94:1287–1290. doi: 10.2138/am.2009.3287
769 [Pan D, Spanu L, Harrison B, Sverjensky DA, Galli G et al](#) (2013) Dielectric properties of water under

Formattato: Pedice

Formattato: Pedice

Formattato: Pedice

Formattato: Pedice

Formattato: Pedice

Formattato: Pedice

Formattato: Pedice

Formattato: Pedice

Formattato: Pedice

Formattato: Pedice

Formattato: Pedice

Formattato: Pedice

Formattato: Pedice

770 [extreme conditions and transport of carbonates in the deep Earth. Proc Natl Acad Sci USA](#)
771 [110:6646–50. doi: 10.1073/pnas.1221581110](#)

772 Pan D, Galli G (2016) The fate of carbon dioxide in water-rich fluids at extreme conditions. *Sci Adv*
773 *2*:e1601278. doi: 10.1126/sciadv.1601278

774 ~~Pan D, Spanu L, Harrison B, et al (2013) Dielectric properties of water under extreme conditions and~~
775 ~~transport of carbonates in the deep Earth. Proc Natl Acad Sci USA 110:6646–50. doi:~~
776 ~~10.1073/pnas.1221581110~~

777 Pettko T, Oberli F, Audétat A, [Guillong M, Simon AC, Hanley JJ, Klemm LM et al](#) (2012) Recent
778 developments in element concentration and isotope ratio analysis of individual fluid inclusions by
779 laser ablation single and multiple collector ICP-MS. *Ore Geol Rev* 44:10–38. doi:
780 10.1016/j.oregeorev.2011.11.001

781 [Poli S. \(2015\) Carbon mobilized at shallow depths in subduction zones by carbonatitic liquids. Nat](#)
782 [Geosci 8, 633–636. doi: 10.1038/ngeo2464](#)

783 Ryabchikov ID, Schreyer W, Abraham K (1982) Compositions of aqueous fluids in equilibrium with
784 pyroxenes and olivines at mantle pressures and temperatures. *Contrib to Mineral Petrol* 79:80–84.
785 doi: 10.1007/BF00376964

786 [Ryabchikov ID, Brey G, Kogarko LN, Bulatov VK \(1989\) Partial melting of carbonatised peridotite at 50](#)
787 [kbar. *Geochem Int* 26:1–7.](#)

788 Sanchez-Valle C, Martinez I, Daniel I, [Philippot P, Bohic S, Simionovici A et al](#) (2003) Dissolution of
789 strontianite at high P-T conditions: An in-situ synchrotron X-ray fluorescence study. *Am Mineral*
790 *88*:978–985.

791 Schmidt MW, Ulmer P (2004) A rocking multianvil: elimination of chemical segregation in fluid-
792 saturated high-pressure experiments. *Geochim Cosmochim Acta* 68:1889–1899. doi:
793 10.1016/j.gca.2003.10.031

794 Schneider ME, Eggler DH (1986) Fluids in equilibrium with peridotite minerals: Implications for mantle
795 metasomatism. *Geochim Cosmochim Acta* 50:711–724. doi: 10.1016/0016-7037(86)90347-9

796 Shmulovich KI, Graham CM, Yardley BWD (2001) Quartz, albite and diopside solubilities in H₂O–NaCl
797 and H₂O–CO₂ fluids at 0.5–0.9 GPa. *Contrib to Mineral Petrol* 141:95–108. doi:
798 10.1007/s004100000224

799 Shmulovich KI, Yardley BWD, Graham CM (2006) Solubility of quartz in crustal fluids: Experiments
800 and general equations for salt solutions and H₂O–CO₂ mixtures at 400–800 °C and 0.1–0.9 GPa.
801 *Geofluids* 6:154–167. doi: 10.1111/j.1468-8123.2006.00140.x

802 Stalder R, Ulmer P, Thompson ~~ABa~~, Günther D (2001) High pressure fluids in the system MgO–SiO₂–
803 H₂O under upper mantle conditions. *Contrib to Mineral Petrol* 140:607–618. doi:
804 10.1007/s004100000212

805 Sverjensky DA, Harrison B, Azzolini D (2014) Water in the deep Earth: The dielectric constant and the
806 solubilities of quartz and corundum to 60 kb and 1200 °C. *Geochim Cosmochim Acta* 129:125–
807 145. doi: 10.1016/j.gca.2013.12.019

808 Tiraboschi C, Tumiati S, Recchia S, [Miozzi F, Poli S et al](#) (2016) Quantitative analysis of COH fluids

Formattato: Pedice

Formattato: Pedice

Formattato: Pedice

Formattato: Pedice

Formattato: Pedice

Formattato: Pedice

Formattato: Pedice

809 synthesized at HP-HT conditions: an optimized methodology to measure volatiles in experimental
810 capsules. *Geofluids* 16:841–855. doi: 10.1111/gfl.12191

811 [Tumiati S, Fumagalli P, Tiraboschi C, Poli S \(2013\) An experimental study on COH-bearing peridotite](#)
812 [up to 3.2 GPa and implications for crust-mantle recycling. *J Petrol* 54, 453–479.](#)

813 [Tumiati S, Tiraboschi C, Sverjensky D, Pettke T, Recchia S, Ulmer P, Miozzi F, Poli S \(2017\) Silicate](#)
814 [dissolution boosts the CO2 concentrations in subduction fluids. *Nat Commun* 8:616. doi](#)
815 [10.1038/s41467-017-00562-z](#)

816 Walther J-V., Long MI (1986) Experimental determination of calcite solubilities in supercritical H₂O. *Int*
817 *Symp Water-Rock Interact* 5:609–611.

818 Walther J-V., Orville PM (1983) The extraction-quench technique for determination of the
819 thermodynamic properties of solute complexes: application to quartz solubility in fluid mixtures.
820 *Am Mineral* 68:731–741.

821 Wolery TJ (1992) EQ3NR, A computer program for geochemical aqueous speciation-solubility
822 calculations: theoretical manual, user's guide and related documentation (version 7.0).

823 [Zhang C, Duan Z \(2009\) A model for C-O-H fluid in the Earth's mantle. *Geochim Cosmochim Acta*](#)
824 [73:2089–2102. doi: 10.1016/j.gca.2009.01.021](#)

825 Zhang C, Duan Z (2010) GFluid: An Excel spreadsheet for investigating C-O-H fluid composition under
826 high temperatures and pressures. *Comput Geosci* 36:569–572. doi: 10.1016/j.cageo.2009.05.008

827 [Zhang C, Duan Z \(2009\) A model for C-O-H fluid in the Earth's mantle. *Geochim Cosmochim Acta*](#)
828 [73:2089–2102. doi: 10.1016/j.gca.2009.01.021](#)

829 Zhang YG, Frantz JD (2000) Enstatite-forsterite-water equilibria at elevated temperatures and pressures.
830 *Am Mineral* 85:918–925.

831

832

Formattato: Pedice